# Electromagnetic Properties of Open and Closed Overmoded Slow-Wave Resonators for Interaction with Relativistic Electron Beams

W. Main, Y. Carmel, *Senior Member, IEEE,* K. Ogura, J. Weaver, G. S. Nusinovich, *Senior Member, IEEE,* S. Kobayashi, J. P. Tate, J. Rodgers, A. Bromborsky, *Member, IEEE,* S. Watanabe, M. R. Amin, K. Minami, W. W. Destler, *Fellow, IEEE,* and V. L. Granatstein, *Fellow, IEEE*

***Abstract*— Specific slow wave structures are needed in order to produce coherent Cherenkov radiation in overmoded relativistic generators. The electromagnetic characteristics of such slow wave, resonant, finite length structures commonly used in relativistic backward wave oscillators have been studied both experimentally and theoretically. In experiments, perturbation techniques were used to study both the fundamental and higher order symmetric transverse magnetic (TM) modes. Finite length effects lead to end reflections and quantization of the wave number. The effects of end reflections in open slow wave structures were found from the spectral broadening of the discrete resonances of the different axial modes. The measured axial and radial field distributions are in excellent agreement with the results of a 2-D code developed for the calculation of the fields in these structures.**

***Index Terms*— Periodic structures, slow waves, dispersion curve, resonators.**

## I. Introduction

VARIOUS electrodynamic structures capable of supporting the propagation of slow electromagnetic waves are widely used for microwave generation and for the acceleration of charged particles. These slow-wave structures are designed to match the phase velocity of the propagating electromagnetic waves to the speed of electrons in the same structure in order to facilitate an effective beam/wave interaction. For interaction with weakly relativistic electron beams it is therefore necessary to slow down the wave's phase velocity significantly while for interaction with relativistic electron beams the phase velocity required is only slightly smaller than the speed of light. The electromagnetic properties of structures with very different phase velocities, obviously, would also be expected to be very different. Therefore, in spite of the availability of detailed studies of structures intended for operation in conventional, weakly relativistic microwave tubes [1], [2] there is still a need for more detailed studies of slow wave structures intended for operation with relativistic electron beams.

A second motivation for the work presented in this paper is the recent interest that has developed around the generation of high power microwave radiation in devices employing overmoded slow wave structures. Despite traditional concerns about mode competition in overmoded devices, recent experiments [3], [4] have shown that efficient, high power operation can be achieved in such devices operating in a single mode. The present study, therefore, has been undertaken in part to accurately determine the electromagnetic characteristics of overmoded slow wave structures to aid in the linear and nonlinear analysis of advanced microwave sources employing such circuits.

Finally, such issues as finite length of the periodic structures and finite reflections at both ends should be studied in more detail. For example, in a finite length structure the axial wave numbers of the electromagnetic modes are quantized affecting the spectral characteristics of device operation. Also, the amount of reflection at both ends of the structure affects the quality factor of each of the quantized axial modes in the multiple resonance "slow-wave" cavity in a unique way. This, in turn, strongly influences the interaction of the electrons with the electromagnetic waves associated with each mode. Especially important is the effect of reflections on the nonstationary operation of short pulse relativistic backward wave oscillators (BWO's) [5], [6].

Perturbation techniques are available for measuring the spatial distribution of fields in resonant cavities [1], [2]. These techniques have been primarily applied to the fundamental modes in accelerator cavities, which are electromagnetically closed (shorted) at both ends and typically have quality factors (Q) over 4000. In contrast, the Q factors of spatially periodic slow-wave structures intended for operation with intense relativistic electron beams are much lower ($\sim$ several hundred) and the electromagnetic properties of these structures have not been studied in detail until recently [7]-[11]. Due to the high fields achieved in these devices, microwave power is usually extracted via open-ended matching sections that lower the total Q and can cause asymmetric axial field distributions. To accurately model this type of device it is important to know the reflection coefficient at the end of the structure and the field

Manuscript received September 30, 1993; revised May 30, 1994. Part of this work was presented as an invited talk at the IEEE ICOPS 1993. This work was supported in part by the Air Force Office of Scientific Research and the Army Research Laboratory.

The authors are with the Institute for Plasma Research, University of Maryland, College Park, Maryland 20742-3511 USA, except as noted:

W. Main is with ACCURAY, Inc., Santa Clara, CA USA.

K. Ogura, S. Watanabe, M.R. Amin, and K. Minami are with Niigata University, Niigata City, Japan.

A. Bromborsky is with Army Research Laboratories, Adelphi, MD USA

IEEE Log Number 9404603D.

0093-3813/94$04.00 © 1994 IEEE

Authorized licensed use limited to: Rochester Institute of Technology. Downloaded on May 13, 2009 at 18:19 from IEEE Xplore. Restrictions apply.

distribution. To date, parameters have usually been obtained through numerical calculations, which are more complicated as the Q-factor decreases. In this study we present experimental methods for determining these parameters and for checking the results of numerical calculations.

To properly address these issues we have developed a formalism describing the fields inside a finite length, spatially periodic structure and methods for measuring the fields and end reflections. For this study we used a periodic structure in the shape of a cylindrical waveguide with a sinusoidally varying conducting wall. A schematic diagram of this apparatus appears in Fig. 1(a). The dispersion diagram for the first six symmetric transverse magnetic modes in an infinitely long slow wave structure with the same dimensions is shown in Fig. 1(b). The periodic nature of the structure leads to a band pass characteristic of each mode. The passbands are given an index, starting with 1 for the lowest and increasing by 1 for each subsequent passband. Thus, the first is referred to as $TM_{01}$, the second as $TM_{02}$, and the nth as $TM_{0n}$. In this paper, we have studied the fundamental ($TM_{01}$) and two higher order ($TM_{02}$, $TM_{03}$) transverse magnetic modes in a spatially periodic, sinusoidally corrugated structure of finite length. Preliminary data for $TM_{04}$ is also available.

This paper is organized as follows. In Section II we discuss the formation of axial modes associated with each transverse mode in a finite length periodic resonator and the relation of these modes to the dispersion diagram of the corresponding infinite length structure. This dispersion diagram is useful for modeling some aspects of BWO operation, such as the relation of beam energy to the approximate operating frequency. To model the more complex nonlinear behavior, it is necessary to numerically simulate the operation of the BWO. For that purpose one needs to know the amplitude and phase of the reflection coefficient from the structure ends, as well as the beam-wave coupling coefficient. The coupling coefficient can only be calculated once the field profile in the structure is known. In Section III we describe how the electromagnetic fields are calculated by expanding the fields in a spatially harmonic series. In Section IV we show how the resonant frequencies as well as the radial field profile associated with each axial mode of the closed slow-wave structure was measured for the three TM modes considered. In Section V we describe how we experimentally determined the reflection coefficient at the open end of our slow-wave resonator. This was done by measuring the spectral width of each resonance, which broadens as the end of the slow-wave resonator is opened. We present both experimental and numerical results for the end reflection. Section VI summarizes our work and describes our latest efforts to increase the accuracy of our results. Possible extensions of these techniques to plasma filled systems are also discussed. Two appendices are also attached to explain the calculation of the reflection coefficient and the analytic model used for the closed cavity quality factor.

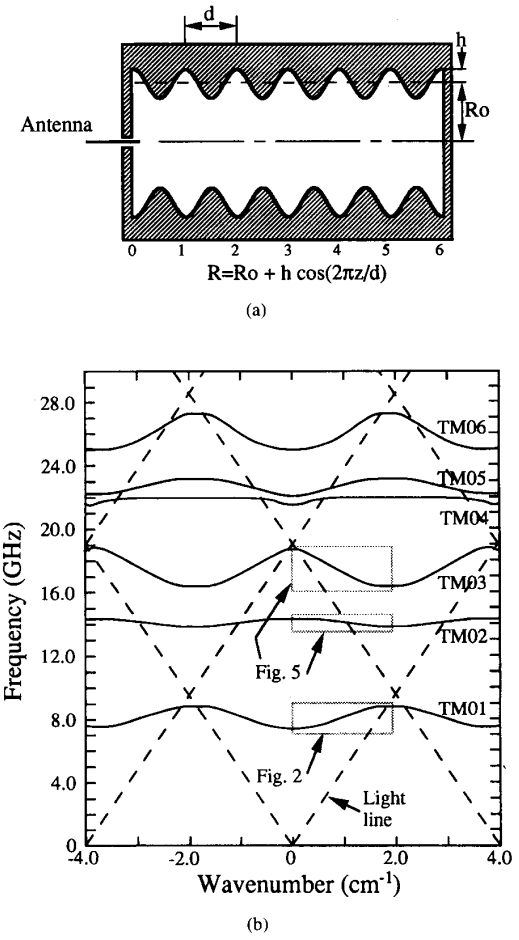


Fig. 1. (a) Schematic diagram of a spatially periodic (corrugated wall) structure shorted at both ends. (b) The calculated dispersion diagram for six symmetric transverse magnetic ($TM_{0s}$) modes in an infinitely long, spatially periodic structure of Fig.1(a).

## II. Axial Modes in a Finite Length Slow-Wave Cavity

The dispersion characteristics of electromagnetic modes in an infinitely long spatially periodic structure are determined only by the geometry of the conducting walls. A finite length structure, however, can be described by a simple dispersion relation only when it is well matched at both ends (i.e., no reflections). Structures used in relativistic BWO's are usually not well matched. First, relativistic BWO's utilize a strong reflection at the entrance of the structure to prevent microwave propagation into the diode region [7], [8], [10], [11]. At the output end of the structure, part of the microwave radiation is reflected and part transmitted. As a result of these reflections a standing wave pattern is created leading to a spectrum of axial modes. This effect was studied in [5] and [6].

Any spatially periodic structure with end reflections containing $N$ periods will support $N + 1$ different axial modes for each transverse mode [12]. Each of these axial modes is characterized by a discrete frequency ($f_r$) and a discrete axial wave number ($\beta_r$), which are located on the dispersion curve of the same transverse mode in an otherwise identical structure of infinite length. As a consequence of the spatial periodicity of the structure, traveling waves can be presented as a super

Authorized licensed use limited to: Rochester Institute of Technology. Downloaded on May 13, 2009 at 18:19 from IEEE Xplore. Restrictions apply.

position of spatial harmonics. The standing wave is formed by a pair of such traveling waves propagating in opposite directions. As an example, the measured frequencies and wave numbers of the seven axial modes associated with the lowest order symmetric transverse magnetic mode ($TM_{01}$) of the six period slow-wave structure of Fig. 1 are shown in Fig. 2(a). In Fig. 2(a) we show, for simplicity, only axial wave numbers for the forward wave in the zero's Brillouin zone. Bear in mind that for a given frequency, the total field contains a set of axial wave numbers corresponding to different spatial harmonics. Throughout this paper, resonance plots will be presented as frequency (in GHz) versus the normalized wave number, $\beta d$, which is equal to the phase advance per structure period. Here $\beta$ is the axial wave number and $d$ is the length of the structure period. The structure wall radius is given by

$$R_w = R_0 + h\cos(2\pi z/d) \tag{1}$$

where $R_0$ is the average radius and $h$ is the amplitude of the wall corrugations. Even though all seven axial modes shown belong to the same transverse magnetic mode ($TM_{01}$), they are characterized by completely different patterns of field lines. As an example, the calculated electric field line pattern of two of the seven axial modes in the slow-wave structure of Fig. 1 are shown in Fig. 2(b). The technique used to calculate these patterns will be described in Section III.

A few features of finite length structures follow from Fig. 2(a), which describes an X-band slow-wave structure having a passband from 7.4 to 8.7 GHz for the fundamental symmetric transverse magnetic ($TM_{01}$) mode. First, the discrete axial modes which are equally spaced in wave number are not equally spaced in frequency within the structure passband. The mode separation varies between 0.05 and 0.25 GHz for the structure studied in this work. Second, the spectral resonance width (and thus the quality factor) of each of the axial modes is different since the group velocity of the electromagnetic wave varies. This feature is used to calculate the end reflection of shorted and open slow-wave structures, as will be shown in Section V.

In addition to the dispersion curve, Fig. 2(a) shows all seven $TM_{01}$ resonance peaks for a closed six-period slow-wave cavity as measured with a microwave network analyzer. For a structure with $N$ periods of length $d$ the resonance condition can be stated as [12]

$$Nd = (n_r/2)(2\pi/\beta) \tag{2}$$

where $n_r$ is the number of half wavelengths along the axis of the structure and $(2\pi/\beta)$ is the axial wave length. The resonant axial wave number $\beta_r$ is then found from $n_r$ using the above equation. Points on the dispersion curve are found by recording the resonant frequencies $f_r$ and associated axial wave numbers $\beta_r$ for the set of axial modes associated with each transverse magnetic (TM) mode. The complete dispersion relation can then be constructed from these discrete points [13] or calculated, as will be shown in Section III. Measuring the

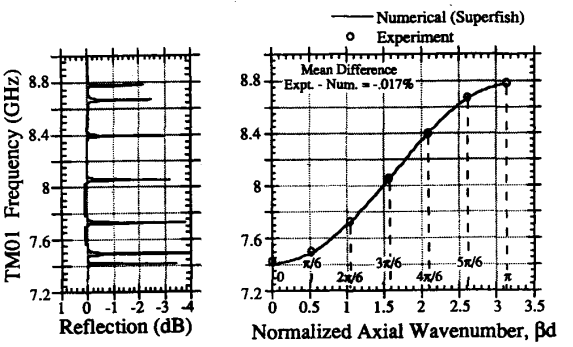


(a)

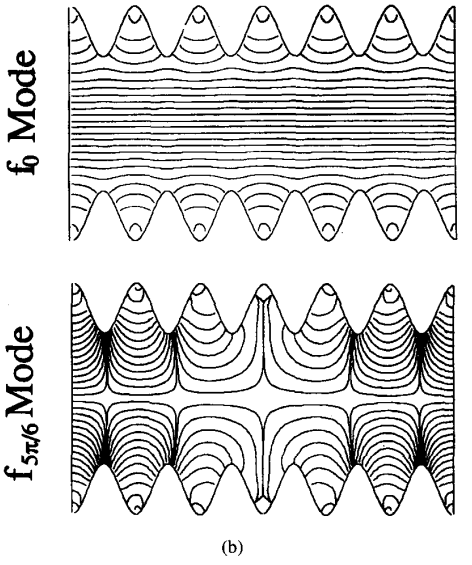


(b)

Fig. 2. (a) The dispersion diagram of an X-band slow wave structure having a passband of 7.4 to 8.7 GHz for the $TM_{01}$ mode as calculated by Superfish, presented as a smooth line. Only half of the first Brillouin zone is shown. Also shown is the measured reflection data and all seven $TM_{01}$ resonance peaks of the closed six period slow wave cavity (open circles). (b) The electric field line pattern associated with two of the seven axial modes (0,5$\pi$/6).

dispersion relation is therefore reduced to finding the set of resonant frequencies and axial wave numbers ($f_r$, $\beta_r$) for the desired TM mode. In practice it is much easier to find the frequencies than the wave numbers. For a spatially periodic resonator excited by an ideal mode launcher, the $N+1$ axial modes associated with a single TM mode should be equally spaced in wave number. Thus if the dispersion curve, $f(\beta)$, is known to be an increasing or decreasing monotonic function of the wave number over one Brillouin zone, then it is necessary to measure only the resonance frequencies. If the dispersion relation is non-monotonic, then it is necessary to measure both $f$ and $\beta$ to determine $f(\beta)$. In this study we consider the fundamental ($TM_{01}$) and the next two higher order ($TM_{02}$ and $TM_{03}$) transverse modes, which are monotonic; however, the techniques presented also apply to nonmonotonic modes. In Section IV we show how these resonances were measured.

Authorized licensed use limited to: Rochester Institute of Technology. Downloaded on May 13, 2009 at 18:19 from IEEE Xplore. Restrictions apply.

## III. Numerical Modeling of the Slow-Wave Structure Fields

### A. Field model

The first step in the simulation of overmoded slow wave structures is to find a way to accurately and efficiently calculate the electromagnetic fields in the structure. As higher modes are considered, these calculations become more complex and it becomes also important to experimentally verify the results. Here we present a technique which shows good agreement with experimental measurements for closed, spatially periodic structures at least up to the $TM_{03}$ mode.

We use a model [14]–[16] in which the fields are expanded in a spatially harmonic series, according to Floquet's theorem. Solving the dispersion relation for the sinusoidal boundary of the slow-wave structure given by (1) gives the expansion coefficients. Using Maxwell's equation, we get the following expressions for the electromagnetic field components, $E_z$, $E_r$, and $H_\phi$,

$$E_z(r,z,t) = \sum_{n=-\infty}^{\infty} A_n J_0\left(\frac{\chi_n}{R_0} r\right) e^{i(\beta_n z - \omega t)} \tag{3}$$

$$E_r(r,z,t) = -iR_0 \sum_{n=-\infty}^{\infty} \frac{A_n \beta_n}{\chi_n} J_1\left(\frac{\chi_n}{R_0} r\right) e^{i(\beta_n z - \omega t)} \tag{4}$$

$$H_\phi(r,z,t) = -i\epsilon_0 \omega R_0 \sum_{n=-\infty}^{\infty} \frac{A_n}{\chi_n} J_1\left(\frac{\chi_n}{R_0} r\right) e^{i(\beta_n z - \omega t)} \tag{5}$$

where $J_0$ and $J_1$ are the Bessel functions of the first kind of order 0 and 1, respectively,

$$\chi_n^2 = R_0^2(\omega^2/c^2 - \beta_n^2) \tag{6}$$

where $\beta_n = \beta + n2\pi/d$ is an integer and $c$ is the velocity of light in vacuum. The dispersion relation is derived from the boundary condition [17] requiring that the tangential electric field is zero at the wall $r = R(z)$,

$$E_t(R) \propto E_z(R) + E_r(R)dR/dz = 0. \tag{7}$$

The spatial Fourier transform of (7) can be expressed as:

$$D \cdot A = 0 \tag{8}$$

where $A$ is a coefficient vector in (3)-(5) and $D$ is a matrix of infinite order. The dispersion relation is the non-trivial solution of (8) and is given by

$$\det\left[D(\beta,\omega)\right] = 0. \tag{9}$$

In the case of a finite length, slow-wave structure, the additional boundary conditions at both ends ($z = 0$ and $z = L$) must be satisfied [18]. A wave propagating forward along the z-axis, $F$, reflects at $z = L$ and becomes a backward propagating wave $B$. Fig. 3(a) illustrates this process, and

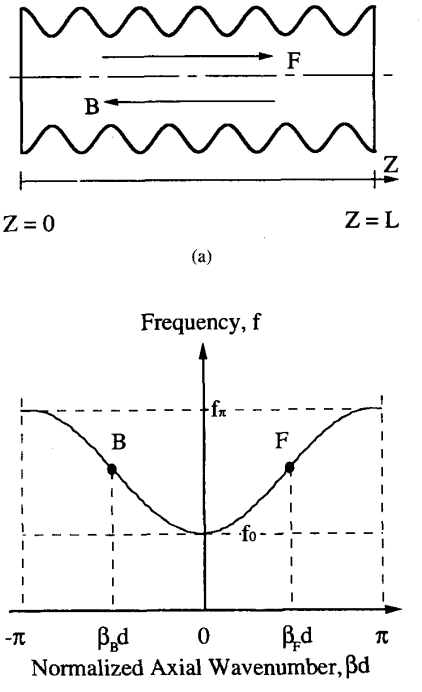


Fig. 3. (a) A wave propagating forward along the z-axis, $F$, reflects at $z = L$ and becomes a backward propagating wave. (b) The location of the $F$ and $B$ waves on the dispersion diagram.

Fig. 3(b) shows the location of these waves on a dispersion diagram.

Both forward and backward waves have to satisfy the dispersion relation,

$$\det\left[D(\beta_F,\omega)\right] = 0, \tag{10}$$

$$\det\left[D(\beta_B,\omega)\right] = 0. \tag{11}$$

Electromagnetic quantities must also be single valued at a given position and time at the resonance,

$$\rho e^{\{i(\beta_F - \beta_B)L\}} = 1. \tag{12}$$

Here, $\rho$ is a round trip reflection coefficient. With the assumption of a loss less cavity that is completely shorted at both ends, we may write $\rho = 1$ and $\beta_B = -\beta_F$. Hence, (12) becomes

$$\beta_F = \pi N/L \tag{13}$$

where $N$ is an integer. Except for the propagation direction, the backward wave is identical to the forward wave; that is, it satisfies the same radial boundary condition and has the same energy. Therefore, in (3)-(5), the relationship between the coefficients $A_n^B$ of backward wave and those $A_n^F$ of the forward wave may be written as

$$A_n^F = A_{-n}^B. \tag{14}$$

By summing the forward and backward waves, the electromagnetic field components in the cavity can be written

$$E_z(r,z,t) = e^{-i\omega t} \sum_{n=-\infty}^{\infty} 2A_n J_0\left(\frac{\chi_n}{R_0} r\right) \cos(\beta_n z) \tag{15}$$

Authorized licensed use limited to: Rochester Institute of Technology. Downloaded on May 13, 2009 at 18:19 from IEEE Xplore. Restrictions apply.

$$E_r(r,z,t) = R_0 e^{-i\omega t} \sum_{n=-\infty}^{\infty} \frac{2A_n\beta_n}{\chi_n} J_1\left(\frac{\chi_n}{R_0} r\right) \sin(\beta_n z) \tag{16}$$

$$H_\phi(r,z,t) = -i\epsilon_0\omega R_0 e^{-i\omega t} \sum_{n=-\infty}^{\infty} \frac{2A_n}{\chi_n} J_1\left(\frac{\chi_n}{R_0} r\right) \cos(\beta_n z). \tag{17}$$

In our calculations, the rank of the matrix was truncated at 9 ($-4 < n < 4$) [15], [16]. Once the dispersion relation, (9), is solved numerically, the ratios of the coefficients, $A_n/A_o$, are determined from (8). With a known set of $A_n/A_o$, the field components $E_z$, $E_r$, and $H_\phi$ are calculated from (15)-(17).

### B. Perturbation Theory

Perturbation theory indicates that slight changes in the shape of a resonant cavity can affect the resonant frequency. Each resonance (associated with an axial mode) is frequency shifted by a perturbing object of volume $\Delta V$ by a different amount. The general relation for the relative frequency shift is given by [2]

$$\frac{\Delta f_r}{f_r} = \frac{\int_{\Delta V} (\mu H \cdot H^* - \epsilon E \cdot E^*) dV}{\int_V (\mu H \cdot H^* + \epsilon E \cdot E^*) dV} \tag{18}$$

where the integral in the numerator is evaluated over the perturbing object volume $\Delta V$ and the integral in the denominator is evaluated over the whole cavity. This assumes that the perturbing object is small compared to the amplitude and length of the wall ripple. For the case of a sphere [2] the above equation is geometrically corrected by multiplying the first term in the numerator by 3/2 and the second term in the numerator by 3. For a small metal bead of radius $r_0$ the field is almost constant over $\Delta V$ so the integration is unnecessary. Thus the equation commonly used is [1]

$$\frac{\Delta f_r}{f_r} = 2\pi r_0^3 \left(\frac{1}{2} H_0^2 - E_0^2\right) \tag{19}$$

where $E_0$ and $H_0$ are the field amplitudes normalized so that the integral of $H_0^2$ or $E_0^2$ over the cavity is unity. Since the only field component on axis is $E_z$, the simplest measurement would be to find $\beta_r$ by perturbing the field on axis. In our experiment, a bead was placed 0.54 cm away from the axis because of the difficulty associated with having both the bead and the antenna on axis. At this radius it was still possible to identify $\beta_z$ for the $TM_{01}$ modes by inspection of the axial profile of the frequency shift. Once the cavity fields are calculated, (19) can be used to find the associated perturbation. This frequency shift can then be directly compared with experimental measurements.

## IV. Results of the Field Model and Experimental Verification

There are two levels at which we can compare the field model of Section III with experiment. The first and simplest level is to compare the measured and calculated resonant frequencies associated with the axial modes. The second is to compare the field distribution (or the related spatial distribution of frequency shifts) of these modes using the spatial perturbation technique described in Section III. In this section we will present the comparison on both levels. Fig. 4 shows the measurement system, including the bead-pull apparatus to be described later.

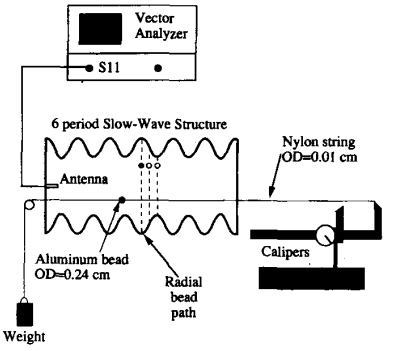


Fig. 4. Cold test system used for measuring the electromagnetic characteristics of spatially periodic structures. The perturbing bead could be translated both axially and radially.

### A. Resonant Frequencies

Experimentally, the modes of our slow-wave structure were excited using a small Hertzian antenna on the axis which could be moved axially in and out of the cavity to adjust the degree of coupling and to enable calibration. A network analyzer was used to measure the microwave reflection from the cavity over the desired frequency range ($S_{11}$ single port measurement). The resonances appeared as narrow spikes at frequencies where the magnitude of the reflection was reduced.

The experimental results appear as plots of the resonant frequency ($f_r$) versus the normalized axial wave number ($\beta d$). All measurements were compared with numerical calculation. The measurements agree very well with the boundary specific calculation of Section III and the general boundary calculation using the 2-D electromagnetic code Superfish [19]. A graphical comparison of the experimental results with Superfish calculations is shown in Fig. 2(a). This figure shows the dispersion curve and reflection data with a common frequency axis. The Superfish results, which were actually calculated at seven points, are converted to form a smooth curve to aid in comparison with experiment. Similar plots comparing the measured and calculated results [16], [20] for the $TM_{02}$ and $TM_{03}$ modes are shown in Fig. 5(a) and 5(b), respectively. The measured frequencies of the $TM_{01}$ resonances are, on average, 0.17% lower than our calculations and 0.03% higher than Superfish. For the $TM_{02}$ and $TM_{03}$ modes the experimental data are, respectively, 0.05% and 0.37% lower than our calculations.

### B. Field Distribution

To perturb the cavity a small object had to be placed at known locations within the structure and the resulting shift in the frequency of a given resonant mode was measured. Fig. 4 shows a schematic diagram of the apparatus and Table I gives a few critical dimensions.

Authorized licensed use limited to: Rochester Institute of Technology. Downloaded on May 13, 2009 at 18:19 from IEEE Xplore. Restrictions apply.

TABLE I
DIMENSIONS OF SLOW-WAVE STRUCTURE.

| | |
|---|---|
| Structure Period | 1.67 cm |
| Total Length | 10 cm (6 periods) |
| Radius [cm] | $1.5 + .41 \sin(3.7z)$ |
| Bead Diameter | 0.24 cm |
| Radial Position of String | 0.54 cm |

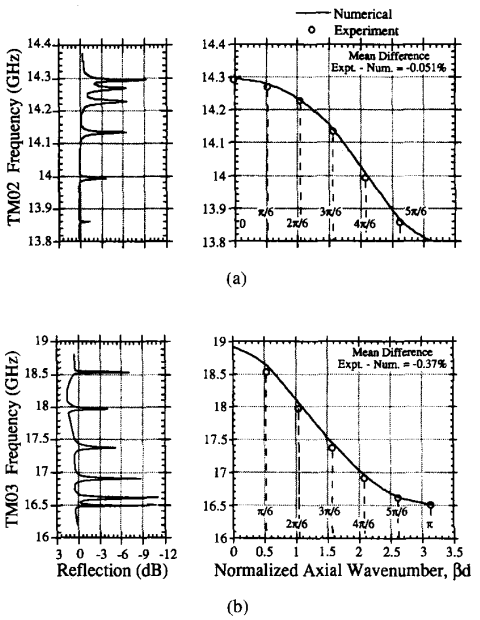


Fig. 5. (a) The dispersion diagram of an X-band slow wave structure having a passband of 7.4 to 8.7 GHz for the $TM_{02}$ mode (smooth line). Also shown is the measured reflection data for the $TM_{02}$ resonance peaks of the closed six period slow wave cavity (open circles). (b) Same as (a), but for the $TM_{03}$ mode.

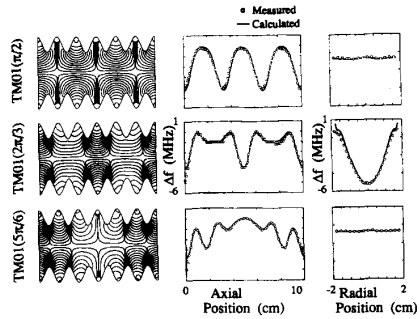


Fig. 6. Field perturbation results in the shorted structure for three axial modes of the $TM_{01}$ transverse mode. (a) Plots of the electric field lines, axial and radial frequency perturbation for $\pi/2$ axial mode; solid lines - calculation based on equation 18; open circles - experiment. (b) Same, for $2\pi/3$. (c) Same, for $5\pi/6$.

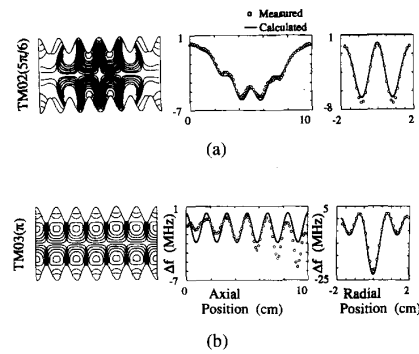


Fig. 7. Field perturbation results of the shorted structure for one axial mode of high order transverse modes. (a) Plots of the electric field lines, axial and radial frequency perturbation for $5\pi/6$ axial mode of the $TM_{02}$ mode; solid lines - calculation based on (18); open circles - experiment. (b) Same, for $\pi$ mode of the $TM_{03}$ transverse mode.

An aluminum bead was suspended in the cavity on a nylon thread via one of four sets of access holes: one set parallel to the cavity axis and three along the diameter at axial positions corresponding to the maximum, average, and minimum radii of the slow wave structure. Bead movement was regulated by tying one end of the thread to a dial caliper to measure position and the other end to a small weight to provide tension. An HP network analyzer measured the forward and reflected power versus frequency ($S_{11}$) from a coax Hertzian element inserted on axis through the cavity end plate. For each mode, the resonant frequency was recorded as a function of bead position. The frequency shift at a given point is then the difference between this frequency and the frequency in an unperturbed cavity. It should be noted that the effect of the nylon thread was negligible (less than 500 kHz in all cases). Both axial and radial dependence of frequency shifts were measured. The first shift was measured with the bead translated along a path parallel to the cavity axis at a radial position of 0.54 cm. The second shift corresponded to a radial path at a position of maximum cavity diameter (see Fig. 4).

In general, measurements and calculations can be performed for each of the seven axial modes associated with each of the three transverse modes ($TM_{01}$, $TM_{02}$, $TM_{03}$). In Fig. 6 and 7 we present selected results. All seven axial modes of the $TM_{01}$ group of modes and some of the axial modes of the $TM_{02}$, $TM_{03}$, and $TM_{04}$ have been studied numerically and experimentally. The results are shown in Fig. 6(a), (b), (c) for the $TM_{01}$ $\pi/2$, $TM_{01}$ $2\pi/3$, and $TM_{01}$ $5\pi/6$ modes, respectively. The experimental results appear as circles overlaid on solid lines that represent the numerical results. To help visualize the cavity fields, a plot of the electric field lines for each axial mode is displayed beside the corresponding data. Similarly, Fig. 7(a) displays the $5\pi/6$ mode of the $TM_{02}$ series and Fig. 7(b) shows the $\pi$ mode of the $TM_{03}$ series. The normalized wave number, $\beta d$, can be found from these results by simply counting the number of local maxima along the length of the resonator and multiplying the number by $\pi/6$.

## V. REFLECTION AND Q-FACTOR OF AN OPEN SLOW-WAVE STRUCTURE

In most low power linear microwave devices the output power is extracted radially at one end of the interaction region. Microwave mode converters change the cylindrical mode produced in the interaction region into the fundamental

Authorized licensed use limited to: Rochester Institute of Technology. Downloaded on May 13, 2009 at 18:19 from IEEE Xplore. Restrictions apply.

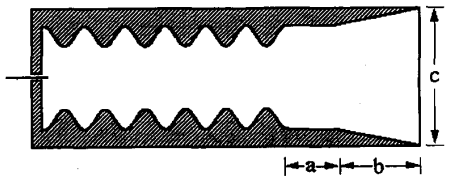


(a)

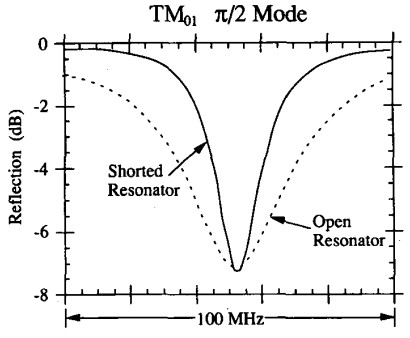


(b)

Fig. 8. (a). A schematic diagram of an open slow wave cavity – a way for axial power extraction in a relativistic backward wave oscillator. In this work $a$ = 1.02 cm, $b$ = 7.62 cm, $c$ = 4.75 cm. (b). Demonstration of resonance broadening. The $\pi/2$ resonance of the $TM_{01}$ mode is broadened when the structure is open (dotted line) as compared to the shorted case (solid). This effect is used to calculate the reflection at the end of the structure.

mode of a waveguide which can transport the energy to the load or antenna. At power levels of tens of MW, the complex geometry of the mode converter can lead to breakdown even in vacuum. To avoid this problem high power tube designs eliminate the mode converter and allow the output power to exit the slow-wave structure along the beam axis. Then the beam is separated from the microwave by tapering the magnetic guide field and thus dumping the beam into the wall of the waveguide. For these discussions this type of cavity is labelled "open" [23]. A diagram of a practical open cavity used in high power BWO experiments [8], [11] is shown in Fig. 8(a).

When modeling a BWO it is important to know the end reflection of the structure. End reflections affect both the starting conditions and saturation effects in the device [5], [6]. Several numerical codes can predict the end reflection coefficient ($\rho$) for a given geometry, however, it is often difficult to accurately calculate end reflections due to the complex geometry of such systems and the often unknown surface finish conditions used. For these reasons it is important to perform experimental measurements. The most direct method of measuring $\rho$ is to launch the desired mode down the structure and measure the waves which are transmitted through or reflected from the end of the structure. This technique requires both launching the desired mode and completely absorbing the reflected wave inside the structure. Either of these would be very difficult in practice. It is much easier to find $\rho$ indirectly by exploiting its relation to the diffractive quality factor of the structure. The diffractive quality factor of a structure ($Q_d$) is related to the radiative power loss through the output aperture of the cavity, whereas the power loss to the walls is related to the ohmic quality factor of the cavity ($Q_{\mathrm{ohm}}$).

To find $Q_d$ it is necessary to separate the ohmic losses ($Q_{\mathrm{ohm}}$) from the total circuit losses ($Q_t$) which include the radiative losses of the cavity. Since the Q-factor is inversely related to power loss, $Q_d$ can be found from $Q_t$ and $Q_{\mathrm{ohm}}$ by the relation

$$Q_d = 1/(1/Q_t - 1/Q_{\mathrm{ohm}}). \tag{20}$$

Both $Q_t$ and $Q_{\mathrm{ohm}}$ can be measured directly. The measured quality factor of the system is $Q_t$ when the structure is open, and $Q_{\mathrm{ohm}}$ when the diffractive loss is eliminated by placing a short at the output side of the structure. Fig. 8(b) demonstrates this effect by showing how the $\pi/2$ resonance of the $TM_{01}$ mode is broadened when the end of the structure is opened.

### A. Experimental measurement of Q

It is useful to give some details of our Q measurement here. We measured the voltage standing wave ratio (VSWR) of the cavity across the desired resonance or resonances using a HP8510C vector network analyzer (we used a one-port measurement for simplicity). From this data we found the minimum VSWR (at resonance) and the maximum VSWR (between resonances). From these two values we used a technique [21] to find the VSWR level at which to read the upper and lower frequencies, $f_1$ and $f_2$, of each resonance. From these frequencies, and the resonant frequency $f_r$ we can calculate the cavity Q using the relation

$$Q = f_r/(f_1 - f_2). \tag{21}$$

With the additional knowledge of whether the cavity was under-coupled (less than optimum coupling) or over-coupled (more than optimum coupling) a correction factor for the Q was found that eliminated the loading effect of our measurement apparatus and wave launcher. The cavity coupling could be adjusted by moving the launcher in and out of the cavity. Using the minimum insertion which would give a clear resonance we were certain to be in the under-coupled regime. The cavity was made of brass.

Using these techniques we measured the Q's of the cavity modes in both open-ended and close-ended configurations. As a check we compared the measured Q's for the shorted configuration with an analytic calculation which is described in detail in Appendix II. These results appear in Fig. 9. The agreement of the measured and calculated Q's is very good when we use a surface roughness factor of 1.7. This factor effectively increases the skin depth in the calculation to compensate for increased field penetration due to surface imperfections (i.e. fabrication, oxidation).

We use (20) to calculate $Q_d$ from the measured values of $Q_t$ and $Q_{\mathrm{ohm}}$. The only remaining step is to calculate the end reflection, $\rho$, from $Q_d$. Appendix I presents a derivation of the

Authorized licensed use limited to: Rochester Institute of Technology. Downloaded on May 13, 2009 at 18:19 from IEEE Xplore. Restrictions apply.

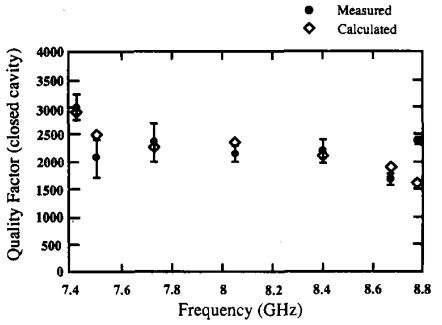


Fig. 9. Calculation (open squares) and measurement (bars) of the wall losses for various axial modes associated with the $TM_{01}$ mode of the shorted periodic cavity. The surface finish factor is 1.7.

relation of these two parameters. The result is

$$\rho = \sqrt{\frac{1-(\alpha/Q_d)}{1+(\alpha/Q_d)}} \tag{22}$$

where $\alpha = (\omega/c)^2(L/\beta)$. Using this relation the measured values of $\rho$ were found. These values of $\rho$ for the $TM_{01}$ axial modes were compared with a set of calculations performed by A. Bromborsky [22]. The results appear in Fig. 10(b). The measured reflection coefficients are up to 15% larger than the calculated ones. This is a significant difference since reflections are important for both the linear characteristics (starting conditions) and for simulations of non-stationary operation of pulsed relativistic backward wave tubes. For example, a 15% change in the reflection coefficient can cause the starting current to double.

## VI. Summary and Conclusions

The electromagnetic properties of slow-wave resonators for high-power relativistic backward wave tubes have been studied both theoretically and experimentally. The agreement between the measured and calculated frequencies and spatial field distributions is very good (the discrepancy is less than 0.2%) for the first three symmetric transverse magnetic modes ($TM_{0p\ell}$) with the index $p$ from 1 to 3 and various axial indices $\ell$ (from 0 to $N$ where $N$ is the number of periods of a slow-wave resonator). Preliminary data is also available for the $TM_{04}$ mode, which is characterized by a very flat dispersion curve (see Fig. 1).

We have also developed a simple method to measure the end reflections in open slow-wave resonators by measuring their Q-factors. This measurement technique gives results for end reflections which are up to 15% higher than those that follow from computer code simulations [22].

Applying these techniques is especially important to high-power relativistic BWO's with overmoded structures because their dispersion diagram may not be a monotonic function of the axial wave number. For this reason it is necessary to measure both the frequency and the axial wave number, as was done in this work, in order to identify the transverse and axial indices of the operating mode.

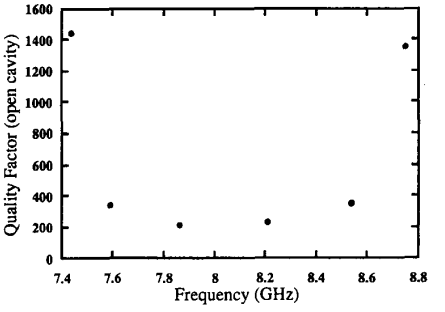


(a)

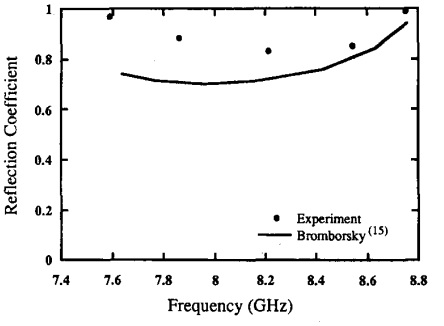


(b)

Fig. 10. (a) Measurement of the diffractive quality factor of the open periodic cavity for various axial modes associated with the $TM_{01}$ mode. (b) The measured reflection coefficient for various axial modes, derived from the diffraction quality factor using (22).

The results obtained are important in the design of future high-power relativistic backward wave oscillators, relativistic travelling wave tubes, overmoded multiwave Cherenkov and multiwave diffraction generators. We also plan to extend the technique described here to the study of plasma filled relativistic slow wave devices [24].

## Acknowledgment

The authors gratefully acknowledge discussions with T.M. Antonsen, Jr., B. Levush, A. Vlasov, and H. Guo on the behavior of finite length periodic systems. We also thank D. Cohen and J. Pyle for their assistance with the experiment and ARL personnel for their help and the use of their facilities.

## Appendix I
## Dependence of Cavity End-Reflectionon Diffractive Quality Factor

We consider a cavity consisting of a section of waveguide with a short at one end and a "leaky" aperture (antenna) at the other. We find the dependence of the reflection from this aperture, $\rho$, on the diffractive quality factor of the cavity $Q_d$ in two steps. First, we relate $Q_d$ to the ratio of circulating power to power loss, and then we relate this ratio to the end-reflection. We begin with a description of $Q_d$ and how it relates

Authorized licensed use limited to: Rochester Institute of Technology. Downloaded on May 13, 2009 at 18:19 from IEEE Xplore. Restrictions apply.

to the total and ohmic quality factors. These three Q-factors are defined as follows:

$Q_{\text{ohm}}$ = Q-factor related to RF power lost in the cavity wall by resistive heating

$Q_t$ = Q-factor related to all power loss mechanisms (ohmic and radiation)

$Q_d$ = Q-factor related to power lost by diffraction through an aperture in the cavity.

By definition, the Q-factor is related to the cavity power loss, $P_{\text{loss}}$, by the equation

$$Q = \omega(U/P_{\text{loss}})$$

where $\omega$ is the resonant frequency and $U$ is the electromagnetic energy stored in the cavity. Because $Q$ is inversely related to power loss, and the total power loss is equal to the sum of the diffractive and ohmic losses, the three Q-factors have the relation

$$1/Q_t = 1/Q_{\text{ohm}} + 1/Q_d. \tag{23}$$

An experimental measurement of the open cavity would give the value for $Q_t$. If the aperture was shorted then the measurement would give $Q_{\text{ohm}}$. Thus, using this equation, all three $Q$s can be experimentally determined.

We now proceed to relate $Q_d$ to the end reflection. To accomplish the first step we use the relation between power and energy in an empty waveguide

$$P/u = (\beta/\omega)c^2 = v_{gr} \tag{24}$$

where $u$ is the energy per unit length in the waveguide ($U/L$) and $v_{gr}$ is the group velocity. Using this relation the definition of quality factor becomes

$$Q_d = (\omega/c)^2(L/\beta)(P_{\text{circ}}/P_d) \tag{25}$$

where $P_{\text{circ}}$ now represents the power circulating in the cavity. To relate $P_{\text{circ}}/P_d$ to the end-reflection $\rho$, we consider the forward and reverse waves in the cavity with associated power $P_+$ and $P_-$, and the power lost through the cavity aperture $P_d$. By definition

$$P_-/P_+ = |\rho|^2 \tag{26}$$

and

$$P_+ - P_- = P_d \tag{27}$$

so

$$P_d/P_+ = 1 - |\rho|^2. \tag{28}$$

By eliminating $P_+$ and $P_-$ we relate the power ratio to the reflection coefficient

$$\frac{P_{\text{circ}}}{P_d} = \frac{P_+ + P_-}{P_d} = \frac{1 + |\rho|^2}{1 - |\rho|^2}. \tag{29}$$

Thus, substituting into the equation for $Q_d$

$$Q_d = \alpha\frac{1 + |\rho|^2}{1 - |\rho|^2} \tag{30}$$

where

$$\alpha = (\omega/c)^2(L/\beta). \tag{31}$$

Inverting this expression in terms of $\rho$, we find

$$\rho = \sqrt{\frac{1 - (\alpha/Q_d)}{1 + (\alpha/Q_d)}}. \tag{32}$$

This is the relation we used to find the cavity end-reflection in Section V of this paper (22).

## APPENDIX II
## OHMIC LOSSES IN RESONATORS WITH CORRUGATED WALLS

Consider a resonator formed by the part of a cylindrical waveguide with corrugated walls which is bounded with two end walls. In general, the ohmic quality factor (Q) of any resonator can be defined as

$$Q_{\text{ohm}} = \frac{\overline{W}}{\overline{W}_{\text{ohm}}} = 2\frac{\int_V \overline{|\vec{H}_\sim|^2}dV}{\int_{V_{\text{skin}}} \overline{|\vec{H}_\sim|^2}dV}. \tag{33}$$

Here, the bars imply the averaging over the wave time period $2\pi/\omega$, $W$ is the microwave energy stored in the resonator, $W_{\text{ohm}}$ is the microwave energy concentrated in a skin-layer of the metallic walls. $V_{\text{skin}}$ is the volume associated with the skin depth. The coefficient 2 reflects the fact that inside a resonator the electric field amplitude is equal to the magnetic field amplitude while in a metallic wall (with the finite but very large conductivity, $\sigma$) only the magnetic field is significant since $E_\sim \sim (1/\sqrt{\sigma})H_\sim$.

We will restrict our consideration to the simplest but most important case of symmetric $\text{TM}_{0p\ell}$ modes. The magnetic field of such modes has only one, non-zero component directed along azimuthal coordinate $\phi$ ($H_{\sim\phi}$). In a corrugated structure with strong end reflections this field, excited at the given frequency $\omega$, can be presented as

$$H_{\sim\phi} = H_\phi e^{i\omega t} + \text{ complex conjugate.}$$

where

$$H_\phi = i\epsilon_0\omega R_0 \sum_{n=-\infty}^{\infty} \frac{A_n}{\chi_n} J_1(g_n r)e^{i\beta_n z} \tag{34}$$

$$\beta_n = l\pi/L + n\bar{\beta}$$

Here $l\pi/L$ is the axial wave number of the field, the wave number $\bar{\beta}$ is determined by the period of corrugation $d$: $\bar{\beta} = 2\pi/d$, the transverse wave number $g_n$ is equal to $g_n = [(\omega/c)^2 - \beta_n^2]^{1/2}$. This is the form given by (5). For slow spatial harmonics $g_n^2 < 0$ ($n \neq 0$), and therefore, $J_1(g_n r) = iI_1(p_n r)$

Authorized licensed use limited to: Rochester Institute of Technology. Downloaded on May 13, 2009 at 18:19 from IEEE Xplore. Restrictions apply.

where $p_n^2 = -g_n^2$. Below we will take into account only zero and $\pm$ first spatial harmonics supposing that amplitudes of all other harmonics are negligibly small.

Let us consider periodical corrugation of the resonator wall,

$$R = R_0 + h \cdot cos\bar{\beta}z \tag{35}$$

and suppose that the height of these ripples, $h$, is much smaller than the wavelength, $\lambda$. In such a case of small ripples it is possible to replace the boundary condition for the field at the real corrugated wall by an approximate boundary condition at the wall of the cylindrical waveguide of radius $R_0$ [25]. From this condition one can find the relation between spatial harmonic amplitudes [26]:

$$\frac{A_{\pm 1}}{A_0} = -i\frac{h}{2} \cdot \frac{g_0^2 \mp (l\pi/L) \cdot \bar{\beta}}{p_{\pm 1}} \cdot \frac{J_1(g_0 R_0)}{I_0(p_{\pm 1} R_0)}. \tag{36}$$

In the case of arbitrary relations between h and $\lambda$ the ratio of harmonic amplitudes can be found only numerically.

In addition to the assumptions given above let us also assume that the structure consists of an integer number of periods: $L = N \cdot d$ where $N$ is an integer. Then, for the microwave energy stored in the resonator one can obtain the following formula:

$$\overline{W} = \pi L R_0^2 \left[\left(\epsilon_0 \omega R_0 \frac{A_0}{\chi_0}\right) J_1(\chi_p)\right]^2 \left(1 + \alpha_1^2 \phi_1 + \alpha_{-1}^2 \phi_{-1}\right) \tag{37}$$

where $\chi_p = g_0 R_0$ is the $p$th root of the equation $J_0(\chi) = 0$, which is the boundary condition for the $TM_{0p\ell}$ mode in a waveguide of the constant radius $R_0$,

$$\begin{aligned} \alpha_{\pm 1} &= \left(\frac{h}{2} \cdot \frac{g_0^2 \mp l\pi/L \cdot \bar{\beta}}{p_{\pm 1}}\right), \pm \\ \pm & \\ \phi_{\pm 1} &= \tfrac{1}{I_0^2(p_{\pm 1} R_0)} \left[I_1^2(p_{\pm 1} R_0) - I_0(p_{\pm 1} R_0) I_2(p_{\pm 1} R_0)\right]. \end{aligned} \tag{38}$$

The last two terms in (II.5) correspond to the $\pm$ first spatial harmonics.

In a similar manner one can find the microwave energy stored in a skin-layer of the depth $\delta_{sk}$. Note that due to a certain roughness of the wall, a realistic skin depth is 1.5 – 2 times larger [27] than the theoretical value. Correspondingly, the ohmic Q-factor of the closed cavity

$$Q_{\text{ohm}}^{\text{closed}} = \frac{\overline{W}}{\overline{W}_{\text{ohm,corr}} + \overline{W}_{\text{ohm,e.w.}}} \tag{39}$$

where $\overline{W}_{\text{ohm,corr}}$ is the average microwave energy concentrated in a skin- layer of the corrugated wall of a waveguide section, and $\overline{W}_{\text{ohm,e.w.}}$ is the microwave energy concentrated in a skin-layer of end walls. Denoting the skin-depth by $\delta_{sk}$ one can derive for $\overline{W}_{\text{ohm,corr}}$, $\overline{W}_{\text{ohm,e.w.}}$ the following expressions:

$$\begin{aligned} \overline{W}_{\text{ohm,corr}} &= \pi \delta_{sk} L \left(\epsilon_0 \omega R_0 \tfrac{A_0}{\chi_0}\right)^2 R_0 J_1^2(\chi_p) \\ &\left\{1 + \alpha_1^2 q_1^2 + \alpha_{-1}^2 q_{-1}^2 + \tfrac{h}{R_0}(\alpha_1 q_1 + \alpha_{-1} q_{-1}) + \left(\tfrac{h\bar{\beta}}{2}\right)^2\right\}, \end{aligned} \tag{40}$$

$$\begin{aligned} \overline{W}_{\text{ohm,e.w.}} &= 2\pi \delta_{sk} \left(\epsilon_0 \omega R_0 \tfrac{A_0}{\chi_0}\right)^2 R_0^2 J_1^2(\chi_p) \\ &\left\{1 + \alpha_1^2 \phi_1 + \alpha_{-1}^2 \phi_{-1} + 4\alpha_1 \tfrac{p_1}{\bar{\beta} + 2(l\pi/L)} \cdot \tfrac{1}{\bar{\beta} R_0}\right. \\ &\left. + 4\alpha_{-1} \tfrac{p_{-1}}{\bar{\beta} - 2(l\pi/L)} \tfrac{1}{\bar{\beta} R_0} + \tfrac{\alpha_1 \alpha_{-1}}{\bar{\beta} R_0 \cdot (l\pi/L)} (p_1 q_{-1} - p_{-1} q_1)\right\}, \end{aligned} \tag{41}$$

Here $q_{\pm 1}$ denotes $I_1(p_{\pm 1} R_0)/I_0(p_{\pm 1} R_0)$.

Substituting equations (II.5), (II.6), (II.8) and (II.9) into (II.7) one can find the ohmic Q-factor of the closed cavity. In microwave generation experiments [3,4,6,7] structures without end walls are used. Correspondingly, when reflections of the microwave power at both ends ($z = 0$ and $z = L$) are large enough, the ohmic Q-factor of the resonator can be estimated by the following equation

$$Q_{\text{ohm}}^{\text{open}} = \frac{\overline{W}}{\overline{W}_{\text{ohm,corr}}}, \tag{42}$$

where $\overline{W}$ and $\overline{W}_{\text{ohm,corr}}$ are defined by Eqs. (II.5) and (II.8), respectively. Equation (II.7) was used in Section V (and Fig. 9) to calculate the ohmic losses in a shorted cavity.

Two limiting cases should be considered separately. In case of the 0-mode, we have $l = 0, \beta_1^2 = \beta_{-1}^2, p_1 = p_{-1}, q_1 = q_{-1}, \alpha_1 = \alpha_{-1}$ and $\phi_1 = \phi_{-1}$, which means that the first and minus first harmonics degenerate to each other except for difference in propagating direction. Thus we have to recalculate our formulas from the first step by taking the degeneracy into consideration. This leads to simplified expressions for terms defined by eqs.(II.8),(II.9). We do not present here these formulas because it was found that for parameters of our slow-wave structure the amplitudes of $\pm$ first harmonics are small ($A_1 = A_{-1} = 0.02A_0$), and therefore these harmonics can be ignored in calculation. This fact has been used to calculate the Q-value of the 0-mode in Fig. 6.

In case of $\pi$-mode, a zero harmonic of forward wave and minus first harmonic of backward wave have the same axial wave number as well as a zero harmonic of backward wave and plus first harmonic of forward wave. They propagate in opposite directions and thus form a standing wave together. In other words, these harmonics degenerate to each other in terms of dependence of the radial coordinate and therefore all formulas must account for this effect. We do not present here these formulas recalculated, because it was found that in our experiment the intersection between the light-line, $\omega = k_z c$ and the dispersion curve is close to the point of the $\pi$-mode, which means $\mid g_0 \mid \ll \bar{\beta}$, where

$$p_0^2 \equiv -g_0^2 = -\left(\frac{\omega}{c}\right)^2 + \frac{\bar{\beta}^2}{4} > 0.$$

This condition $\mid g_0 \mid \ll \bar{\beta}$ simplifies the consideration. For experimental parameters the following relation between har-

Authorized licensed use limited to: Rochester Institute of Technology. Downloaded on May 13, 2009 at 18:19 from IEEE Xplore. Restrictions apply.

monic amplitudes was found,

$$\frac{A_1}{A_0} = -1.57 \times 10^{-4}, \qquad \frac{A_{-1}}{A_0} = 1.025.$$

Thus we were able to ignore the plus first harmonic and to approximate the magnetic field as

$$H_\phi = \left(\epsilon_0 \omega R_0 \frac{A_0}{\chi_0}\right) I_1(p_0 R_0) cos(\bar{\beta} z/2) \qquad (43)$$

This expression has been used to calculate the Q-value of the $\pi$-mode in Fig. 6.

## REFERENCES


[1] L. C. Maier and J. C. Slater "Field strength measurements in resonant cavities," *J. Appl. Phys.*, vol. 23, pp. 68-77, 1952.

[2] Om. P. Gandhi, *Microwave Engineering and Applications*, Pergamon Press, 1984.

[3] D. K. Abe, T. Antonsen, Jr., Y. Carmel, W. W. Destler, V. L. Granatstein, B. Levush, and S. M. Miller, "Experimental studies of overmoded high power microwave generators," in *1993 IEEE Inter. Conf. on Plasma Science.*

[4] D. K. Abe, T. Antonsen, Jr., A. Bromborsky, Y. Carmel, B. Levush, and S. M. Miller, "Experimental and theoretical results from the University of Maryland multiwave Čerenkov generator program," in *Beams '92 Conf. Proc.*

[5] B. Levush, T. M. Antonsen, Jr., A. Bromborsky, W. R. Lou, Y. Carmel, "Theory of relativistic backward wave oscillators with end reflections," *IEEE Trans. Plasma Sci.*, vol. 30, pp. 263-280, 1992.

[6] B. Levush, T. M. Antonsen, Jr., A. Bromborsky, W. R. Lou, Y. Carmel, "Relativistic backward wave oscillators: Theory and experiment," *Phys. Fluids B*, vol. 4, pp. 1-7, 1992.

[7] N. F. Kovalev, M. I. Petelin, M. D. Raiser, A. V. Smorgonsky and L. E. Tsopp. "Generation of powerful electromagnetic radiation pulses by a beam of relativistic electrons," *JETP Lett.*, vol. 18, pp. 138-140, 1973.

[8] Y. Carmel, W. R. Lou, J. Rodgers, H. Guo, W. W. Destler, V. L. Granatstien, B. Levush, T. Antonsen, Jr., and A. Bromborsky, "From linearity towards chaos: Basic studies of relativistic backward wave oscillators," *Phys. Rev. Lett.*, vol. 69, pp. 1652-1655, 1992.

[9] S. P. Bugaev et al., "Relativistic multiwave Cerenkov generators," *IEEE Trans. Plasma Sci.*, vol. 18, pp. 525-536, 1990.

[10] S. D. Korovin *et al.*, "The nonuniform-phase velocity relativistic BWO," in *9th International Conference on High Power Particle Beams, BEAMS 92*, Washington, DC, May 25-29, 1992, Paper PG-02.

[11] R. A. Kehs *et al.*, "High power backward wave oscillator driven by a relativistic electron beam," *IEEE Trans. Plasma Sci.*, vol. PS-13, pp. 559-562, 1985.

[12] C. C. Johnson, *Field and Wave Electrodynamics*, New York: McGraw-Hill, 1965, ch. 7.

[13] Y. Carmel, H. Guo, W. R. Lou, D. Abe, V. L. Granatstein, and W. W. Destler, "Novel method for determining the electromagnetic dispersion relation of periodic slow wave structures," *Appl. Phys. Lett.*, vol. 57, pp. 1304-1306, 1990; also, H. Guo, Y. Carmel, W. R. Lou, L. Chen, J. Rodgers, D. Abe, A. Bromborsky, W. Destler, and V. L. Granatstein, "A novel highly accurate technique for determination of the dispersive characteristics in periodic slow wave circuits," *IEEE Trans. Microwave Theory and Tech.*, vol. 40, pp. 2086-2094, 1992.

[14] J. A. Swegle *et al.*, "Backward wave oscillators with rippled wall resonators: Analytic theory and numerical simulation," *Phys. Fluids*, vol. 28, pp. 2882-2894, 1985. This paper also contains a list of Soviet references on this topic.

[15] K. Minami, Y. Carmel, V. L. Granatstein, W. Destler, W. R. Lou, D. Abe, T. Hosokawa, K. Ogura, and T. Watanabe, "Linear theory of electromagnetic wave generation in plasma loaded corrugated wall resonators," *IEEE Trans. on Plasma Sci.*, vol. 18, pp. 537-545, 1990.

[16] K. Ogura, K. Minami *et al.*, *J. Phys. Soc. Japan*, vol. 61, p. 3966, 1992.

[17] V.I. Kurilko *et al.*, *Sov. Physics Tech. Physics*, vol. 24, p. 1451, 1979.

[18] M.M. Ali, K. Ogura *et al.*, *Phys. Fluids B*, vol. 4, p. 1023, 1992.

[19] K. Halbach, and R. Holsinger, *Part. Accel.*, vol. 1, p. 213, 1976.

[20] The results are also in excellent agreement with those of A. Bromborsky and B. Ruth, *IEEE Trans. Microwave Theory Tech.*, vol. MTT-32, p. 600, 1984.

[21] D. K. King, *Measurement at Centimeter Wavelength*, pp. 128-141, New York: Van Nostrand Co., 1952. See also, L. Malter and G. A. Brewer, *J. Appl. Phys.*, vol. 20, p. 10, 1949.

[22] A. Bromborsky, private communication.

[23] The subject of "open" cavities with smooth walls is discussed in L.A. Weinstein, *Open Resonators and Open Waveguides*, Boulder, CO: Golem Press, 1969. In this work we deal with cavities having spatially periodic walls.

[24] Y. Carmel, W. R. Lou, T. M. Antonsen, Jr., J. Rodgers, B. Levush, W. W. Destler, and V. L. Granatstein, "Relativistic plasma microwave electronics: Studies of high-power plasma filled backward wave oscillators," *Phys. Fluids B*, vol. 4, pp. 2286-2292, 1992.

[25] N. F. Kovalev, "Electrodynamic structure of the ultrarelativistic BWO," *Elektronnaya Tekhnika*, ser. 1, Electronika SVCh, no. 3, pp. 102-106, 1978.

[26] B. Z. Katzenelenbaum, *Theory of Irregular Waveguides with Slowly Variable Parameters*, Moscow, 1961.

[27] K. Kreisher and R.J. Temkin, in *Infrared and Millimeter Waves*, vol. 7, ch. 8, Academic Press, 1983, p. 377.


**William Main,** photograph and biography not available at the time of publication.

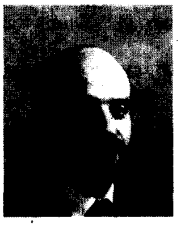

**Yuval Carmel** (S'66-M'74) was born in Israel in 1942. He received the B.Sc. (EE) and M. Sc. (EE) degrees from the Technion, Israel Institute of Technology, in 1966 and 1971, respectively, and the Ph.D.(EE) degree from Cornell University, Ithaca, NY, in 1974.

He was with the government of Israel, the Naval Research Laboratory, and is currently with the University of Maryland, College Park. His research interest include electromagnetic radiation from intense electrons beams, plasma microwave devices, advanced concepts in millimeter-wave tubes, gyrotrons, and backward wave oscillators.

**K. Ogura** was born in Japan in 1957. He received the B.Sc. degree in physics from Okayama University in 1981, and the M.Sc. and D.Sc. degrees in physics from Kyoto University in 1983 and 1989, respectively.

He is an Associate Professor in the Electrical and Electronic Engineering Department of Niigata University. His research interests include high-power microwave oscillators and their applications to plasma heating.

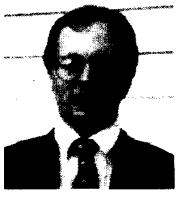

**James Weaver** received the B.S. degree in physics from the Massachusetts Institute of Technology in 1992. He is currently a graduate student in the Department of Electrical Engineering at the University of Maryland at College Park.

Authorized licensed use limited to: Rochester Institute of Technology. Downloaded on May 13, 2009 at 18:19 from IEEE Xplore. Restrictions apply.

**Gregory Nusinovich** for a photograph and biography see page 524 of this issue.

**S. Kobayashi** received the B.Sc. and M.Sc. degrees in geological science from Kyoto University, in 1986 and 1989, respectively, and the M.Sc. degree in physics from Washington State University in 1991. He is currently a graduate student in the Department of Physics at the University of Maryland, College Park.

**Jeffrey P. Tate** was born on April 15, 1958 in Detroit, Michigan. He received the B.S. degree in electrical engineering in 1982 from Michigan State University, East Lansing. From 1982-1983 he worked as a systems engineer for the Detroit Edison Company. He received the M.S. degree in electrical engineering from Michigan State in 1985. In 1991 he received the Ph.D. degree in electrical engineering and applied physics from Cornell University.

During his study for the M.S. degree, he completed thesis work on magnetostatic surface-wave amplifiers. In 1986 and 1987 he held summer internships with the Advanced Microwave and Millimeter-wave Laboratory of TRW, performing research in the area of gallium-arsenide microwave integrated circuits. His doctoral research involved the characterization of high electron-cyclotron harmonic radiation from a Penning discharge plasma. He currently holds a research associate position at the University of Maryland, College Park, where his work includes the study of advanced harmonic gyrotron devices. His other interests include passive microwave components, plasma diagnostics and microwave materials processing.

**John Rodgers**, photograph and biography not available at the time of publication.

**A. Bromborsky**, photograph and biography not available at the time of publication.

**S. Watanabe** was born in Japan in 1969. He received the B.S. (EE) and M.S. (EE) degrees from Niigata University in 1991 and 1993, respectively.

He is presently a Ph.D. candidate at the Graduate School of Science and Technology, Niigata University. His research interests include high-power microwave generators and cryogenic plasmas.

**M. R. Amin** was born in Rangpur, Bangladesh in 1959. He received the B.Sc. (EEE) degree from the University of Rajshahi in 1984 and the M.Sc. (EEE) degree from Bangladesh University of Engineering and Technology, Dhaka, in 1987. He is now on sabbatical from the Bangladesh Institute of Technology, Rajshahi, where he is an Assistant Professor in the Electrical and Electronic Engineering Department. He is presently working toward the Ph.D. degree at the Graduate School of Science and Technology, Niigata University, Japan.

His research interests include theoretical and experimental investigations of high-power microwave devices, and semiconductor power electronic drives.

Mr. Amin is a member of the Institute of Engineers Bangladesh (IEB), and the Physical Society of Japan.

**K. Minami** was born in Japan in 1938. He received the B.S. (EE) degree at Nagoya Institute of Technology in 1962, the M.S. (EE) degree at the Tokyo Institute of Technology in 1964, and the Ph.D. degree at Nagoya University in 1969.

Since 1986 he has been a Professor in the Electrical Engineering Department, Niigata University, Japan. His research interests include the generation of high-power microwave radiation and interaction between powerful microwaves and plasmas.

**William W. Destler** (M'84), photograph and biography not available at the time of publication.

**Victor L. Granatstein** for a photograph and biography see page 525 of this issue.

Authorized licensed use limited to: Rochester Institute of Technology. Downloaded on May 13, 2009 at 18:19 from IEEE Xplore. Restrictions apply.